

Precession of Magnetically Driven Warped Disks and Low-Frequency QPOs in Low-Mass X-Ray Binaries

Akiko Shirakawa and Dong Lai

Center for Radiophysics and Space Research, Cornell University, Ithaca, NY 14853

Email: shirak,dong@astro.cornell.edu

ABSTRACT

An accretion disk around a rotating magnetized star is subjected to magnetic torques which induce disk warping and precession. These torques arise generically from interactions between the stellar field and the induced surface currents on the disk. Applying these new effects to weakly magnetized ($B \sim 10^7\text{--}10^9$ G) neutron stars in low-mass X-ray binaries, we study the global hydrodynamical warping/precession modes of the disk under the combined influences of relativistic frame dragging, classical precession due to the oblateness of the neutron star, and the magnetic torques. Under quite general conditions, the magnetic warping torque can overcome the “Bardeen-Petterson” viscous damping and makes the modes grow. The modes are confined to the inner region of the disk, and have frequencies equal to $0.3 - 0.95$ (depending on the mass accretion rate \dot{M}) times the sum of the Lense-Thirring frequency, the classical precession frequency, and the magnetically driven precession frequency evaluated at the inner disk radius r_{in} . As \dot{M} increases, the mode frequency is reduced relative to the total precession frequency at r_{in} since the mode becomes less concentrated around r_{in} due to the increasing viscous stress associated with the large \dot{M} . Because of this, and because the magnetically driven precession is retrograde (opposite to the Lense-Thirring precession) and depends strongly on \dot{M} , the mode frequency can have a non-monotonic dependence on the mass accretion rate. This may account for several observed features of low-frequency (10–60 Hz) quasi-periodic oscillations (LFQPOs) in low-mass X-ray binaries which are otherwise difficult to explain, such as the flattening/turnover in the LFQPO frequency – \dot{M} correlation or in the LFQPO frequency – kHz QPO frequency correlation (e.g., as seen clearly in GX 17+2).

Subject headings: accretion disks – stars: neutron – stars: magnetic fields – X-rays: binaries – binaries: close

1. Introduction

Accreting neutron stars (NSs) in low-mass X-ray binaries (LMXBs) exhibit rapid, quasi-periodic oscillations (QPOs) in their X-ray fluxes. The so-called horizontal-branch oscillations (HBOs), discovered in a subclass of LMXBs called Z sources, are low-frequency QPOs (LFQPOs) with centroid frequencies in the range of 15–60 Hz, Q -values of order a few, and rms amplitudes $\lesssim 10\%$ (see van der Klis 1995 for a review). One interpretation of the HBOs is the magnetospheric beat-frequency model (Alpar & Shaham 1985; Lamb et al. 1985) in which the HBO frequency is identified with the difference frequency between the Keplerian frequency at the magnetospheric boundary and the spin frequency of the NS. However, over the last few years, the discovery of kilohertz (300–1300 Hz) QPOs in ~ 20 LMXBs by the *Rossi X-Ray Timing Explorer* (*RXTE*) has called into question this interpretation of the HBOs (see van der Klis 2000 for a

review). In particular, observations indicate that in most Z sources, kHz QPOs (which often come in pairs) occur simultaneously with the HBOs. In several atoll sources (which are thought to have weaker magnetic fields and smaller accretion rates than the Z sources), similar LFQPOs have also been found at the same time when kHz QPOs occur. While the origin of the kHz QPOs is still being debated, it is convenient (as in all current theoretical models; see van der Klis 2000 and references therein) to associate one of the kHz peaks with the orbital motion in the inner edge of the accretion disk. On the other hand, the discovery of nearly coherent oscillations during X-ray bursts in several LMXBs establishes the spin frequency of the NS to be $\sim 300\text{--}600$ Hz (see Strohmayer 2000). Obviously, the beating between the kHz orbital frequency and the spin frequency cannot produce the 10–60 Hz LFQPOs.

Stella & Vietri (1998) suggested that the LFQPOs are associated with the Lense-Thirring precession of the inner accretion disk around the rotating NS. If the LFQPO and the kHz QPOs are generated at the same special radius in the disk, this implies a quadratic relation between the LFQPO frequency and the kHz QPO frequency, in rough agreement with observations (usually for certain range of X-ray fluxes; but see §4.4). For reasonable values of NS moment of inertia, the data require that the observed LFQPO peaks correspond to 2 or 4 times the Lense-Thirring frequency (Stella & Vietri 1998; Ford & van der Klis 1998; Psaltis et al. 1999); this may be possible since a precessing disk may induce X-ray flux variation mainly at the harmonics of its fundamental precession frequency and there may be “sub-harmonic” feature buried in the X-ray power spectra (see Jonker et al. 2000).

There are several theoretical and observational puzzles associated with the Lense-Thirring interpretation of LFQPOs. First, it is well-known that the combined effects of differential precession and viscosity tend to keep the inner region of the disk [within $\sim (100 - 1000)GM/c^2$] perpendicular to the NS spin axis (Bardeen & Petterson 1975). A mechanism to drive the disk tilt is then needed for the precession to make sense. Second, because different “rings” in the disk have different precession rates and are strongly coupled to each other, a global mode analysis is needed to determine the true precession rate of the inner disk. Marković & Lamb (1998) carried out such an analysis but found that all the modes are damped even when the radiation driven warping torque (Pringle 1996) is included. Third, pure Lense-Thirring precession has difficulty in explaining the observed behavior of the LFQPO frequency as a function of the accretion rate of the system (Wijnands et al. 1996; Psaltis et al. 1999; see §4.4).

In this paper, we show that the magnetically driven warping instability (Lai 1999), resulting from interactions between the weakly magnetized ($\sim 10^8$ G) NS and the inner accretion disk (see §2), can naturally overcome the Bardeen-Petterson viscous damping and therefore induces a tilt in the inner disk. By carrying out a global analysis of disk precession/warping modes, including magnetic torques in addition to the Lense-Thirring and classical precession torques, we obtain, for the first time, growing warping/precession modes of the disk (see §3 and §4). Moreover, we show that the magnetically driven precession torque (Lai 1999; see §2) significantly affects the actual disk precession frequency as the accretion rate increases; this can potentially explain the observed \dot{M} -dependent behaviors of the LFQPOs (§4).

2. Magnetically Driven Warping and Precession

It is known that if the accretion disk is slightly tilted from the equatorial plane of a rotating neutron star, it precesses due to general relativistic frame-dragging effect (Lense-Thirring precession) and also due to oblateness of the rotating star (classical precession). For a magnetized neutron star, there is an additional magnetically driven precession and warping of the disk; these arise from interactions between

the stellar magnetic field and the disk before the latter is truncated at the magnetospheric boundary (Lai 1999). The magnetic torques appear under the generic condition that the stellar magnetic field (treated as a dipole in this paper) is not aligned with the stellar spin axis. Depending on how the disk responds to the stellar field, two different kinds of torque arise: (i) If the vertical stellar magnetic field B_z penetrates the disk, it gets twisted by the disk rotation to produce an azimuthal field $\Delta B_\phi = \mp \zeta B_z$ that has different signs above and below the disk (ζ is the azimuthal pitch of the field line and depends on the dissipation in the disk), and a radial surface current K_r results. The interaction between K_r and the stellar B_ϕ gives rise to a vertical force. While the mean force (averaging over the azimuthal direction) is zero, the uneven distribution of the force induces a net *warping torque* which tends to misalign the angular momentum of the disk with the stellar spin axis. (ii) If the disk does not allow the vertical stellar field (e.g., the rapidly varying component of B_z due to stellar rotation) to penetrate, an azimuthal screening current K_ϕ will be induced on the disk. This K_ϕ interacts with the radial magnetic field B_r and produces a vertical force. The resulting *precessional torque* tends to drive the disk into retrograde precession around the stellar spin axis.

In general, both the magnetic warping torque and the precessional torque are present. For small disk tilt angle β (the angle between the disk normal and the spin axis), the warping rate and precession angular frequency at radius r are given by (see Lai 1999)

$$\Gamma_m(r) = \frac{\zeta \mu^2}{4\pi r^7 \Omega(r) \Sigma(r)} \cos^2 \theta, \quad (1)$$

and

$$\Omega_m(r) = -\frac{\mu^2}{\pi^2 r^7 \Omega(r) \Sigma(r) D(r)} \sin^2 \theta, \quad (2)$$

where μ is the stellar magnetic dipole moment, θ is the angle between the magnetic dipole axis and the spin axis, $\Omega(r)$ is the orbital angular frequency, and $\Sigma(r)$ is the surface density of the disk. The dimensionless function $D(r)$ is given by

$$D(r) = \max(\sqrt{r^2/r_{\text{in}}^2} - 1, \sqrt{2H(r)/r_{\text{in}}}), \quad (3)$$

where $H(r)$ is the half-thickness and r_{in} is the inner radius of the disk.

Here we apply these magnetic torques to LMXBs containing weakly magnetized ($B \sim 10^8$ G) NSs. We parametrize the properties of the inner disk using the “inner region” (radiation- and-scattering dominated) solution of α -disk (Shakura & Sunyaev 1973)¹, with

$$\Sigma(r) = (1050 \text{ g cm}^{-2}) \alpha_{-1}^{-1} M_{1.4}^{-1/2} \dot{M}_{17}^{-1} r_6^{3/2} \mathcal{J}(r)^{-1}, \quad (4)$$

$$H(r) = (1.1 \text{ km}) \dot{M}_{17} \mathcal{J}(r), \quad (5)$$

where $\alpha = (0.1) \alpha_{-1}$ is the α -viscosity, $M = (1.4 M_\odot) M_{1.4}$ is neutron star’s mass, $\dot{M} = (10^{17} \text{ g s}^{-1}) \dot{M}_{17}$ is the mass accretion rate and $r_6 = r/(10^6 \text{ cm})$. The dimensionless function $\mathcal{J}(r)$ is given by ²

$$\mathcal{J}(r) = 1 - \xi \sqrt{\frac{r_{\text{in}}}{r}}, \quad (6)$$

¹Such a disk is unstable against thermal-viscous perturbations (see Frank et al. 1992), although the situation is not clear when there are magnetic fields threading the disk. Note that our main results related to the dimensionless mode frequencies (see §4.1 and §4.2) are not very sensitive to disk models (see Shirakawa & Lai 2001, where general power-law disks are studied).

²Magnetic fields threading the disk can modify $\mathcal{J}(r)$ in a model-dependent way (see Lai 1999 for an example). However, the basic feature can still be approximated by eq. (6).

where ξ is a dimensionless parameter with $0 < \xi < 1$. Substituting equations (4) and (5) into equations (1) and (2), and assuming the Keplerian flow for $\Omega(r)$, we get

$$\Gamma_m(r) = (55.3 \text{ s}^{-1}) \zeta \cos^2 \theta \alpha_{-1} \mu_{26}^2 \dot{M}_{17} \mathcal{J}(r) r_6^{-7}, \quad (7)$$

$$\Omega_m(r) = (-70.4 \text{ s}^{-1}) \sin^2 \theta \alpha_{-1} \mu_{26}^2 \dot{M}_{17} D(r)^{-1} \mathcal{J}(r) r_6^{-7}, \quad (8)$$

where $\mu_{26} = \mu/(10^{26} \text{ G cm}^3)$.

The Lense-Thirring precession angular frequency is given by ³

$$\Omega_{LT}(r) = \frac{2GI_3\Omega_s}{c^2 r^3} = (280 \text{ s}^{-1}) I_{45} \left(\frac{\nu_s}{300 \text{ Hz}} \right) r_6^{-3}, \quad (9)$$

where $I_3 = (10^{45} \text{ g cm}^2) I_{45}$ is the moment of inertia around the spin axis and $\Omega_s = 2\pi\nu_s$ is the spin angular frequency. The classical precession angular frequency is given by

$$\Omega_{cl}(r) = -\frac{3G(I_3 - I_1)}{2r^3} \frac{\cos \beta}{\sqrt{GM}r}, \quad (10)$$

where I_1 is the moment of inertia around the axis perpendicular to the spin. If we approximate the rotating NS as a compressible Maclaurin spheroid (Lai et al. 1993), we have $I_3 = (1/5)\kappa_n M(a_1^2 + a_2^2)$ and $I_1 = (1/5)\kappa_n M(a_2^2 + a_3^2)$, where a_i is the semi-major axis of the spheroid, and κ_n is a dimensionless parameter which depends on the polytropic index (e.g., $\kappa_n=1, 0.81482, 0.65345$ for $n=0, 0.5, 1$, respectively). For slow rotation, with $\hat{\Omega}_s \equiv \Omega_s/(GM/R^3)^{1/2} \ll 1$ (where R is the radius of a nonrotating star of the same mass), the semi-major axis is given by $a_i = R(1 + \epsilon_i)$, with (Lai et al. 1994; Appendix A)

$$\epsilon_1 = \epsilon_2 = \frac{1}{4}\kappa_n \left(1 - \frac{n}{5}\right) \left(\frac{5+n}{3-n}\right) \hat{\Omega}_s^2, \quad (11)$$

$$\epsilon_3 = -\frac{1}{2}\kappa_n \left(1 - \frac{n}{5}\right) \left(\frac{5-3n}{3-n}\right) \hat{\Omega}_s^2. \quad (12)$$

Equations (9) and (10) then become (with $\cos \beta \simeq 1$)

$$\Omega_{LT}(r) = (313 \text{ s}^{-1}) \kappa_n \left[1 + \frac{1}{2}\kappa_n \left(1 - \frac{n}{5}\right) \left(\frac{5+n}{3-n}\right) \hat{\Omega}_s^2\right] \left(\frac{\nu_s}{300 \text{ Hz}}\right) M_{1.4} R_6^2 r_6^{-3}, \quad (13)$$

$$\Omega_{cl}(r) = (-195 \text{ s}^{-1}) \kappa_n^2 \left(1 - \frac{n}{5}\right) \left(\frac{\nu_s}{300 \text{ Hz}}\right)^2 M_{1.4}^{-1/2} R_6^5 r_6^{-7/2}, \quad (14)$$

where $R_6 = R/(10^6 \text{ cm})$. Morsink & Stella (1999) have given exact numerical solutions of Ω_{LT} and Ω_{cl} for a variety of nuclear equations of state. But analytic expressions (13) and (14) provide the dominant contributions, and are adequate for the purpose of this paper.

3. Global Precession/Warping Modes: Equations

Since the precession rates $\Omega_{LT}, \Omega_{cl}, \Omega_m$ depend strongly on r , coupling between different rings is needed to produce a global coherent precession. Such coupling can be achieved through either viscous

³In the strong gravitational field and/or rapid stellar rotation regime, the Lense-Thirring precession (angular) frequency is replaced by the nodal precession frequency $\Omega_{nod} \equiv \Omega - \Omega_\theta$ with Ω the orbital frequency and Ω_θ the vertical frequency. The fractional deviation of Ω_{nod} from Ω_{LT} is of order $\hat{a}(M/r)^{1/2}$ (where $\hat{a} = I\Omega_s/M^2$) and will be neglected in this paper.

stress or bending waves (e.g., Papaloizou & Pringle 1983; Terquem 1998 and references therein). In the viscosity dominated regime, the formalism of Papaloizou & Pringle (1983) can be used (see also Pringle 1992; Ogilvie 2000; Ogilvie & Dubus 2001; note that in the linear regime, the different formalisms of disk warping dynamics are equivalent). We specify a warped precessing disk by the disk normal vector $\hat{\mathbf{l}}(r, t)$. In the Cartesian coordinate, with the z -axis along the NS spin, we write $\hat{\mathbf{l}} = (\sin \beta \cos \gamma, \sin \beta \sin \gamma, \cos \beta)$, with $\beta(r, t)$ the tilt angle and $\gamma(r, t)$ the twist angle. For $\beta \ll 1$, the dynamical warp equation for $\hat{\mathbf{l}}$ (see Lai 1999) reduces to an equation for $W(r, t) \equiv \beta(r, t)e^{i\gamma(r, t)}$:

$$\frac{\partial W}{\partial t} - \left[\frac{3\nu_2}{4r} \left(1 + \frac{2r\mathcal{J}'}{3\mathcal{J}} \right) + \frac{3\nu_1}{2r} (\mathcal{J}^{-1} - 1) \right] \frac{\partial W}{\partial r} = \frac{1}{2} \nu_2 \frac{\partial^2 W}{\partial r^2} + i (\Omega_{LT} + \Omega_{cl} + \Omega_m) W + \Gamma_m W, \quad (15)$$

where ν_2 is the viscosity which tends to reduce the disk tilt. We assume that the ratio of ν_2 to the usual viscosity ν_1 is constant. For α disk, $\nu_1 = \alpha H^2 \Omega$, the viscosity rate is

$$\tau_{\text{visc}}^{-1}(r) \equiv \frac{\nu_2(r)}{r^2} = (16.7 \text{ s}^{-1}) \left(\frac{\nu_2}{\nu_1} \right) \alpha_{-1} M_{1.4}^{1/2} \dot{M}_{17}^2 \mathcal{J}(r)^2 r_6^{-7/2}. \quad (16)$$

To look for global modes we consider solutions of the form $W(r, t) = e^{i\sigma t} W(r)$ with the complex mode frequency $\sigma = (\sigma_r + i\sigma_i)$. It is convenient to define a dimensionless mode frequency $\hat{\sigma} = \sigma \tau_{\text{visc}}(r_{\text{in}})$, where $\tau_{\text{visc}}(r_{\text{in}})$ is given by eq. (16) evaluated at r_{in} , the inner disk radius. Similarly, we define dimensionless quantities:

$$\hat{\Omega}_{LT} \equiv \Omega_{LT}(r_{\text{in}}) \tau_{\text{visc}}(r_{\text{in}}) = 16.8 I_{45} \left(\frac{\nu_s}{300 \text{ Hz}} \right) \left(\frac{\nu_1}{\nu_2} \right) \alpha_{-1}^{-1} M_{1.4}^{-1/2} \dot{M}_{17}^{-2} \mathcal{J}_{\text{in}}^{-2} \left(\frac{r_{\text{in}}}{10 \text{ km}} \right)^{1/2}, \quad (17)$$

$$\hat{\Omega}_{cl} \equiv \Omega_{cl}(r_{\text{in}}) \tau_{\text{visc}}(r_{\text{in}}) = -11.7 \kappa_n^2 \left(1 - \frac{n}{5} \right) \left(\frac{\nu_s}{300 \text{ Hz}} \right)^2 \left(\frac{\nu_1}{\nu_2} \right) \alpha_{-1}^{-1} M_{1.4}^{-1} \dot{M}_{17}^{-2} R_6^5 \mathcal{J}_{\text{in}}^{-2}, \quad (18)$$

$$\hat{\Omega}_m \equiv \Omega_m(r_{\text{in}}) \tau_{\text{visc}}(r_{\text{in}}) = -4.2 \sin^2 \theta \left(\frac{\nu_1}{\nu_2} \right) \mu_{26}^2 M_{1.4}^{-1/2} \dot{M}_{17}^{-1} D_{\text{in}}^{-1} \mathcal{J}_{\text{in}}^{-1} \left(\frac{r_{\text{in}}}{10 \text{ km}} \right)^{-7/2}, \quad (19)$$

$$\hat{\Gamma}_m \equiv \Gamma_m(r_{\text{in}}) \tau_{\text{visc}}(r_{\text{in}}) = 3.3 \zeta \cos^2 \theta \left(\frac{\nu_1}{\nu_2} \right) \mu_{26}^2 M_{1.4}^{-1/2} \dot{M}_{17}^{-1} \mathcal{J}_{\text{in}}^{-1} \left(\frac{r_{\text{in}}}{10 \text{ km}} \right)^{-7/2}, \quad (20)$$

where $D_{\text{in}} \equiv D(r_{\text{in}})$ and $\mathcal{J}_{\text{in}} \equiv \mathcal{J}(r_{\text{in}})$. Note that we can use eq. (13) to obtain more explicit expression of $\hat{\Omega}_{LT}$. Equation (15) can now be reduced to the dimensionless form:

$$\begin{aligned} i\hat{\sigma}W - \left[\frac{3}{4x^{5/2}} \left(1 + \frac{2x\mathcal{J}'}{3\mathcal{J}} \right) + \frac{3}{2x^{5/2}} \left(\frac{\nu_1}{\nu_2} \right) \left(\frac{1}{\mathcal{J}} - 1 \right) \right] \frac{\mathcal{J}_{\text{in}}^2}{\mathcal{J}_{\text{in}}^2} \frac{dW}{dx} \\ = \frac{1}{2x^{3/2}} \frac{\mathcal{J}_{\text{in}}^2}{\mathcal{J}_{\text{in}}^2} \frac{d^2W}{dx^2} + i \left[\frac{\hat{\Omega}_{LT}}{x^3} + \frac{\hat{\Omega}_{cl}}{x^{7/2}} + \frac{\hat{\Omega}_m}{x^7} \frac{D_{\text{in}}}{D} \frac{\mathcal{J}}{\mathcal{J}_{\text{in}}} \right] W + \frac{\hat{\Gamma}_m}{x^7} \frac{\mathcal{J}}{\mathcal{J}_{\text{in}}} W, \end{aligned} \quad (21)$$

where $x \equiv r/r_{\text{in}}$ and $\mathcal{J}' = d\mathcal{J}/dx$.

It is clear from eq. (21) that $\hat{\sigma}$ depends only on five dimensionless parameters $\hat{\Omega}_{LT}$, $\hat{\Omega}_{cl}$, $\hat{\Omega}_m$, $\hat{\Gamma}_m$, and ν_1/ν_2 as well as two dimensionless functions $D(x)$ and $\mathcal{J}(x)$. To obtain σ in physical units we need to know r_{in} . We adopt the simple ansatz:

$$r_{\text{in}} = \max(r_m, r_{\text{ISCO}}), \quad (22)$$

where the magnetosphere radius r_m is given by

$$r_m = 18 \eta \mu_{26}^{4/7} M_{1.4}^{-1/7} \dot{M}_{17}^{-2/7} \text{ km}, \quad (23)$$

(with $\eta \sim 0.5$), and the inner-most stable circular orbit ⁴ r_{ISCO} is given by

$$r_{\text{ISCO}} = 6GM/c^2 = 12.4 M_{1.4} \text{ km}. \quad (24)$$

The critical mass accretion rate $\dot{M}_{17, \text{c}}$ below which $r_{\text{in}} = r_m$ and above which $r_{\text{in}} = r_{\text{ISCO}}$ is obtained by equating eqs. (23) and (24) as:

$$\dot{M}_{17, \text{c}} = 3.7 \eta^{7/2} \mu_{26}^2 M_{1.4}^{-4}. \quad (25)$$

A more elaborate prescription for the inner disk radius when both general relativity and the magnetic field are important is discussed in Lai (1998).

To solve eq. (21) for the complex eigenfunction $W(x)$ and eigenvalue $\hat{\sigma}$, six real boundary conditions are needed. In our calculation, the disk extends from $x_{\text{in}} = 1$ to $x_{\text{out}} = 50$. For large x and large $|\hat{\sigma}|$, equation (21) can be solved analytically, giving

$$W(x) \propto \exp \left[\frac{4\sqrt{2}}{7} (i\hat{\sigma})^{1/2} \mathcal{J}_{\text{in}} x^{7/4} \right], \quad (26)$$

where we should choose the sign of $(i\hat{\sigma})^{1/2}$ so that $W(x) \rightarrow 0$ as $x \rightarrow \infty$. This approximate analytical solution, evaluated at x_{out} , together with its derivative, gives four (real) outer boundary conditions. The inner boundary condition generally takes the form $W'(x_{\text{in}}) = aW(x_{\text{in}})$, with a being a constant. Most of our results in §4 will be based on $a = 0$ (corresponding to zero torque at the inner edge of the disk), although we have experimented with different a 's (see Figs. 1-2) and found that for $|a| \lesssim 1$ our results are unchanged to the extent that there are other parameters in the problem which have greater uncertainties. In numerically searching a mode, we make a guess for the eigenvalue $\hat{\sigma}$ and integrate eq. (21) from x_{out} to x_{in} using the Kaps-Rentrop scheme (Press et al. 1992). We use the globally convergent Newton method to find the correct value of $\hat{\sigma}$ that satisfies the boundary conditions.

4. Numerical Results and Discussion

In this section, we first study numerical properties of equation (21) and then discuss specific cases relevant to accreting NSs in LMXBs.

4.1. Mode Eigenfunction and Eigenvalue

For a given set of parameters $(\hat{\Omega}_{LT}, \hat{\Omega}_{\text{cl}}, \hat{\Omega}_m, \hat{\Gamma}_m)$, equation (21) allows for many eigenmodes. Here we shall focus on the “fundamental” mode which is more concentrated near the inner edge of the disk and has larger $\hat{\sigma}_r$ (global precession frequency) and smaller $\hat{\sigma}_i$ (damping rate) than any other “higher-order” modes (see Fig. 1).

If a mode were infinitely concentrated at the inner radius of the disk, one expects that the mode frequency $\hat{\sigma}_r$ is just the sum of the frequencies evaluated at the inner disk radius, i.e., $\hat{\sigma}_r = \hat{\Omega}_{LT} + \hat{\Omega}_{\text{cl}} + \hat{\Omega}_m$. However, the calculated $\hat{\sigma}_r$ is always smaller than $\hat{\Omega}_{LT} + \hat{\Omega}_{\text{cl}} + \hat{\Omega}_m$ because the mode is not infinitely concentrated but has a finite width.

⁴The correction to r_{ISCO} due to stellar rotation is negligible since $\hat{a} \sim 0.1$ for NSs in LMXBs.

Figure 1 shows the tilt angle $\beta(x, t = 0) = |W(x)|$ associated with the modes for different sets of $(\hat{\Omega}_{LT}, \hat{\Gamma}_m)$. We have set $\hat{\Omega}_{cl} = \hat{\Omega}_m = 0$ (since they play a similar role as $\hat{\Omega}_{LT}$), $\mathcal{J}(x) = 1$, and $\nu_1/\nu_2 = 1$ in eq. (21) for simplicity⁵. We see that as $\hat{\Omega}_{LT}$ and $\hat{\Gamma}_m$ increase, the fundamental modes (solid lines) become more concentrated near the inner radius of the disk. This behavior can be understood heuristically: for a given $\Omega_{LT}(r)$, a larger $\hat{\Omega}_{LT}$ implies smaller viscosity, and thus the coupling between different disk radii is reduced.

Figure 2 shows the mode frequency σ in units of $\Omega_{LT}(r_{in})$, or $\sigma/\Omega_{LT}(r_{in}) = \hat{\sigma}/\hat{\Omega}_{LT}$, as a function of $\hat{\Omega}_{LT}$ for different values of $\hat{\Gamma}_m$ [We again set $\hat{\Omega}_{cl} = \hat{\Omega}_m = 0$, $\mathcal{J}(x) = 1$, and $\nu_1/\nu_2 = 1$]. We see that $\hat{\sigma}_r/\hat{\Omega}_{LT}$ always lies between 0.4 to 0.95 for the relevant ranges of $\hat{\Omega}_{LT}$ (10 to 10^4). The ratio $\hat{\sigma}_r/\hat{\Omega}_{LT}$ increases and approaches unity as $\hat{\Omega}_{LT}$ and $\hat{\Gamma}_m$ increase. This is consistent with the behavior of the mode eigenfunction (see Fig. 1) that a larger $\hat{\Omega}_{LT}$ or $\hat{\Gamma}_m$ makes the mode more concentrated near the inner disk edge.

4.2. Global Warping Instability Criterion

As discussed in §1, differential precession tends to be damped by the ν_2 viscosity. Figure 2(b) shows that $\hat{\sigma}_i/\hat{\Omega}_{LT} = \sigma_i/\Omega_{LT}(r_{in})$ is always positive (which implies damping) for $\hat{\Gamma}_m = 0$ and lies between 0.25 (for $\hat{\Omega}_{LT} = 10$) and 0.04 (for $\hat{\Omega}_{LT} = 10^4$), corresponding to Q value ($Q \approx \sigma_r/\sigma_i$) between 2 and 20 (the high- Q regime was also explored by Markovic & Lamb 1999 where a different disk model was adopted). We see that $\hat{\sigma}_i$ decreases as $\hat{\Gamma}_m$ increases, and becomes negative (implying mode growth) when the ratio $\hat{\Gamma}_m/\hat{\Omega}_{LT}$ is sufficiently large. The numerical values for $\hat{\sigma}_i$ can be approximated by

$$\hat{\sigma}_i = -a\hat{\Gamma}_m + b\hat{\Omega}_{LT}^{0.7}, \quad (27)$$

with $a \sim (0.5 - 1.0)$ and $b \sim 0.5$. For the mode to grow ($\hat{\sigma}_i < 0$) we require

$$\hat{\Gamma}_m \gtrsim \hat{\Omega}_{LT}^{0.7} \iff \text{Global Warping Instability.} \quad (28)$$

For $\dot{M}_{17} < \dot{M}_{17,c}$ [see eq. (25)], so that $r_{in} = r_m$, this condition becomes

$$0.7 \zeta \mu_{26}^{-0.2} \cos^2 \theta \alpha_{-1}^{0.7} I_{45}^{-0.7} M_{1.4}^{0.4} \dot{M}_{17}^{1.5} \left(\frac{\nu_s}{300 \text{ Hz}} \right)^{-0.7} \left(\frac{\nu_1}{\nu_2} \right)^{0.3} \left(\frac{\eta}{0.5} \right)^{-3.85} \gtrsim 1. \quad (29)$$

For $\dot{M}_{17} > \dot{M}_{17,c}$, so that $r_{in} = r_{ISCO}$, we require

$$0.2 \zeta \mu_{26}^2 \cos^2 \theta I_{45}^{-0.7} M_{1.4}^{-4} \dot{M}_{17}^{0.4} \left(\frac{\nu_s}{300 \text{ Hz}} \right)^{-0.7} \left(\frac{\nu_1}{\nu_2} \right)^{0.3} \gtrsim 1. \quad (30)$$

We see that for parameters that characterize accreting NSs in LMXBs the mode growth condition can be satisfied (see §4.3 for specific examples), although not always. In general, high (but not unreasonable) ζ (> a few) and \dot{M}_{17} are preferred to obtain growing modes.

4.3. Dependence of Mode Frequency on \dot{M}

In §4.1 and §4.2, we have seen how $\hat{\Omega}_{LT}$ and $\hat{\Gamma}_m$ affect the dimensionless mode frequency $\hat{\sigma}$ ($= \hat{\sigma}_r + i\hat{\sigma}_i$) while setting $\hat{\Omega}_{cl} = \hat{\Omega}_m = 0$. We have found that $\hat{\sigma}_r$ is smaller than the naively expected value $\hat{\Omega}_{LT}$ for small

⁵ Note the results shown in Figs. 1-2 are not sensitive to \mathcal{J} since \mathcal{J}_{in} has been absorbed in the definitions of dimensionless frequencies, eqs. (17)-(20). See also §4.3.

$\hat{\Omega}_{LT}$ and $\hat{\Gamma}_m$, but becomes closer to $\hat{\Omega}_{LT}$ as $\hat{\Omega}_{LT}$ and $\hat{\Gamma}_m$ increase. We have also found that a sufficiently large $\hat{\Gamma}_m$ tends to make the mode unstable. In this subsection, we consider some specific examples to illustrate the dependence of the mode frequency σ on \dot{M} and other parameters for NSs in LMXBs.

Figure 3 shows the global precession frequency (i.e., $\sigma_r/2\pi$; the real part of the mode frequency in physical units)⁶ as a function of the mass accretion rate for a fixed parameter set [Parameter Set A: $M_{1.4} = 1$, $R_6 = 1$, $n = 1$, $\nu_s = 300$ Hz, $\alpha_{-1} = 1$, $\zeta = 5$, $\sin^2 \theta = 0.1$, $\nu_2/\nu_1 = 1$, $\mu_{26} = 2$, $\eta = 0.5$, $\xi = 0$, and $D(x)$ as given in eq. (3)], for three different cases: (i) only the Lense-Thirring precession is included, (ii) both the Lense-Thirring and classical precessions are included, and (iii) the magnetic precession and warping are included in addition to the Lense-Thirring and classical precessions. It also shows the fiducial precession frequency, ν_{fid} , which is the sum of the considered frequencies evaluated at the inner radius of the disk, i.e., $\nu_{\text{fid}} \equiv (\Omega_{LT}(r_{\text{in}}) + \Omega_{\text{cl}}(r_{\text{in}}) + \Omega_m(r_{\text{in}}))/2\pi$.

The dependence of ν_{fid} on \dot{M} is understood in the following manner. From eqs. (13), (14), and (2), together with eqs. (22)–(24), we find $\Omega_{LT}(r_{\text{in}}) \propto \dot{M}^{6/7}$, $\Omega_{\text{cl}}(r_{\text{in}}) \propto \dot{M}$, and $\Omega_m(r_{\text{in}}) \propto \dot{M}^3$ when $r_{\text{in}} = r_m$, and $\Omega_{LT}(r_{\text{in}}) \propto \dot{M}^0$, $\Omega_{\text{cl}}(r_{\text{in}}) \propto \dot{M}^0$, and $\Omega_m(r_{\text{in}}) \propto \dot{M}$ when $r_{\text{in}} = r_{\text{ISCO}}$. Thus we obtain, for the above three different cases:

$$(i) \nu_{\text{fid}} \propto \mathcal{O}(\dot{M}^{6/7}) \ (\dot{M}_{17} < \dot{M}_{17,c}), \quad \nu_{\text{fid}} \propto \mathcal{O}(\dot{M}^0) \ (\dot{M}_{17} > \dot{M}_{17,c}). \quad (31)$$

$$(ii) \nu_{\text{fid}} \propto \mathcal{O}(\dot{M}^{6/7}) - \mathcal{O}(\dot{M}) \ (\dot{M}_{17} < \dot{M}_{17,c}), \quad \nu_{\text{fid}} \propto \mathcal{O}(\dot{M}^0) \ (\dot{M}_{17} > \dot{M}_{17,c}). \quad (32)$$

$$(iii) \nu_{\text{fid}} \propto \mathcal{O}(\dot{M}^{6/7}) - \mathcal{O}(\dot{M}) - \mathcal{O}(\dot{M}^3) \ (\dot{M}_{17} < \dot{M}_{17,c}), \quad (33)$$

$$\nu_{\text{fid}} \propto \mathcal{O}(\dot{M}^0) - \mathcal{O}(\dot{M}) \ (\dot{M}_{17} > \dot{M}_{17,c}). \quad (34)$$

For Parameter Set A adopted in Fig. 3, the transition from $r_{\text{in}} = r_m$ to $r_{\text{in}} = r_{\text{ISCO}}$ occurs at $\dot{M}_{17,c} = 1.3$ [see eq. (25)].

We see from Fig. 3 that the behavior of the mode frequency $\sigma_r/2\pi$ as a function of \dot{M} is different from that of ν_{fid} for all three cases (i)–(iii). For case (i) and (ii), $\sigma_r/2\pi$ is as small as $\sim 30\%$ of ν_{fid} for high \dot{M} ($\dot{M}_{17} \sim 1.5 - 2.0$) and the dependence of $\sigma_r/2\pi$ on \dot{M} is very different from that of ν_{fid} . This is understood from our discussion in §4.1: The viscosity rate increases (and $\hat{\Omega}_{LT} + \hat{\Omega}_{\text{cl}}$ decreases) as \dot{M} increases [see eq. (16)]; this tends to spread the mode by coupling (through viscous stress) disk rings at different radii, thereby reducing $\sigma_r/2\pi$ relative to ν_{fid} . The increasing importance of viscosity for high mass accretion rate is also expected for case (iii), where additional magnetic effects are included. However, we see from Fig. 3 that $\sigma_r/2\pi$ becomes closer to ν_{fid} when the magnetic warping torque (Γ_m) is included. This is understood from our finding in §4.1 (see Figs. 1–2) that the presence of Γ_m makes the mode more concentrated near the disk inner radius.

Figure 4 shows the mode frequency $\sigma_r/2\pi$ as a function of \dot{M} for three sets of parameters, Set A, B, and C, where $(\mu_{26}, \sin^2 \theta) = (2, 0.1)$, $(2, 0.5)$ and $(4, 0.1)$, respectively, while the other parameters are fixed to the standard values: $M_{1.4} = 1$, $R_6 = 1$, $n = 1$, $\nu_s = 300$ Hz, $\alpha_{-1} = 1$, $\zeta = 5$, $\nu_2/\nu_1 = 1$, $\eta = 0.5$, $\xi = 0$. All of the Lense-Thirring, classical precessions and magnetic precession and warping are included [case (iii)]. For Parameter Set A and B, the inner radius of the disk reaches r_{ISCO} at the same $\dot{M}_{17,c} = 1.3$ [see eq. (25)]. For Parameter Set A, $|\Omega_m(r_{\text{in}})|$ is much smaller than $\Omega_{LT}(r_{\text{in}}) + \Omega_{\text{cl}}(r_{\text{in}})$ for small \dot{M}_{17} although it becomes more important for large \dot{M}_{17} ; thus at $\dot{M}_{17} = \dot{M}_{17,c}$, $\sigma_r/2\pi$ suddenly changes from an increasing function of \dot{M} as given by eq. (33) (with small second and third terms) to a linearly decreasing function of

⁶In Figs. 3–6, we multiply the mode frequency by 4 to facilitate comparison with observations, since the QPOs appear to manifest as harmonics of the fundamental frequency (Stella & Vietri 1998; Psaltis et al. 1999; see also §5).

\dot{M} as given by eq. (34). For Parameter Set B, $|\Omega_m(r_{\text{in}})| \propto \sin^2 \theta$ is 5 times larger than that in Parameter Set A and is important even for small $\dot{M}_{17} < \dot{M}_{17,c}$; thus $\sigma_r/2\pi$ shows a gradual turnover feature according to eq. (33) and becomes a linearly decreasing function of \dot{M} [see eq. (34)] above $\dot{M}_{17,c}$. For Parameter Set C, the inner radius of the disk is always given by r_m for the relevant \dot{M} (since $\dot{M}_{17,c} = 5.2$). As $|\Omega_{\text{cl}}(r_{\text{in}})|$ and $|\Omega_m(r_{\text{in}})|$ are much smaller than $\Omega_{LT}(r_{\text{in}})$, $\sigma_r/2\pi$ is a monotonically increasing function as given by eq. (33) (with small second and third terms).

Figure 5 illustrates the dependence of the mode frequency $\sigma_r/2\pi$ on the polytropic index n and the dimensionless parameter ξ [defined in eq. (6)] (other parameters are the same as in Parameter Set A adopted in Fig. 4). Most nuclear equations of state have effective polytropic index between 0.5 and 1. We see that $\sigma_r/2\pi$ is larger for a stiffer equation of state (smaller n) and a larger ξ , although the dependences are not as strong as on other parameters (cf, Fig. 4).

4.4. Comparison with the Observed Behaviors of LFQPOs

The behavior of σ_r as a function of \dot{M} (see Figs. 3–5) is similar to the features observed for the LFQPOs in LMXBs (see van der Klis 1995, 2000). While for some systems, the LFQPO frequencies increase as the X-ray flux increases, for other systems, a non-monotonic (even opposite) correlation between the QPO frequency and \dot{M} has been observed. As an example, for the Z source GX 17+2, using the position of the source on the X-ray color-color diagram as an indicator of \dot{M} , Wijnands et al. (1996) found that the HBO frequency increases with \dot{M} for small \dot{M} but decreases with further increase of \dot{M} . In the simple model where the LFQPO is identified with the precession frequency at the disk inner radius r_{in} (Stella & Vietri 1998; see §1), the non-monotonic behavior is difficult to explain, even when the classical (retrograde) precession is included ⁷ (see Psaltis et al. 1999; Morsink & Stella 1999). However, we see from Fig. 4 that when we consider global disk modes and include the magnetic effects, a variety of $\sigma_r - \dot{M}$ behaviors are possible. In our model the turnover of the $\sigma_r - \dot{M}$ correlation occurs for two reasons: (1) the magnetically driven retrograde precession $\Omega_m \propto -1/r^7$ becomes more important with increasing \dot{M} [see eqs. (33) & (34)]; (2) the viscous stress becomes more important as \dot{M} increases, and makes the mode less concentrated around r_{in} ; thus σ_r is more reduced from ν_{fid} with increasing \dot{M} . We note that even when magnetic effects are not included [case (i) & (ii)], the “turnover” feature is obtained due to mechanism (2) as explained above (see Fig. 3). However, these modes are highly damped by viscosity. Only the magnetic warping torque can make the mode grow (see Fig. 4).

A related puzzle concerns the correlation between the LFQPO frequency and the higher kilohertz QPO frequency (e.g., Stella & Vietri 1998; Ford & van der Klis 1998; Psaltis et al. 1999; see §1). It was found that for several sources the positive correlation flattens (and even turns over) for large kHz QPO frequencies (and large \dot{M}) (see Homan et al. 2001 for a clear case of such turnover in GX 17+2). Again, this feature is difficult to explain with the simple picture of Lense-Thirring and classical precessions at r_{in} , but can be accounted for qualitatively by our global disk oscillation model with magnetic effects (see Fig. 6; note that we have not tried to vary the model parameters to “fit” the observations). More quantitative comparison between our models and the data require a better understanding of the origin of kHz QPOs (e.g., it is not certain whether the kHz QPO frequency is the Keplerian frequency at r_{in} ; see §5 for other uncertainties expected in real systems).

⁷This is because $\Omega_{LT} \propto r^{-3}$ and $\Omega_{\text{cl}} \propto -r^{-7/2}$ have a similar r -dependence; see eqs. (13) and (14).

5. Concluding Remarks

We have shown in this paper that the inner region of the disk around a weakly magnetized ($\sim 10^8$ G) NS is warped due to magnetic field – disk interactions (see Lai 1999) and therefore must precess under the combined effects of relativistic frame dragging, classical precession (due to the oblateness of the NS) and magnetic torques. We have found growing warping/precession modes of the inner disk and shown that these modes have properties that resemble the 10–60 Hz low-frequency QPOs observed in LMXBs (see §4).

Although our treatments of disk warping/precession go beyond many previous models of QPOs (these models typically identify a QPO frequency as the characteristic frequency of a test mass at certain special radius in the disk; see van der Klis 2000 for a review), they still contain important idealizations. For example, we have assumed the stellar field to be dipolar when considering the magnetic field – disk interactions. This is unlikely to be correct for LMXBs since the disk (with r_{in} only a few stellar radii) can produce significant change in the global field topology even when the intrinsic stellar field is dipolar (see Lai, Lovelace & Wasserman 1999). Observationally, the absence of persistent millisecond pulsation in all known LMXBs but SAX J1808.4–3658 (Wijnands & van der Klis 1998) and the frequency drift of burst oscillations (e.g., Strohmayer 2000; see also Cumming et al. 2001) may imply that the NS does not possess a well-defined dipole field, although a more complex field is possible. Also, we have only studied the linear behavior of the warping/precession modes in this paper. Because of these idealizations and the uncertainties in observations (e.g., it is difficult to determine \dot{M} precisely from observations), more quantitative comparison between the observational data and our theory is premature at present. Nevertheless, the results presented in this paper demonstrate that magnetically driven warping and precession can give rise to a variety of new possibilities for the dynamical behaviors of inner accretion disks around magnetic NSs.

Concerning the observed properties of QPOs, many issues remain unanswered in our paper (and in other related QPO studies): e.g, How does the mode manifest itself as a variation in the X-ray flux? How is the observed QPO amplitude (as large as 15%) produced? One possibility is that the LFQPO is caused by occultation of the central NS by the warped, precessing inner disk. Another issue is that for the observed NS spin rates (based on observations of burst oscillations) and reasonable moment of inertia of the neutron star, the data require that the observed LFQPO corresponds to 2 or 4 times the precession mode frequency (see §1; the fact that the global mode frequency is smaller than the precession frequency at r_{in} exacerbates the problem); while this may be possible, more theoretical study on this issue is needed. Finally, there is an indication (but by no means proven) that some black hole systems display low-frequency QPOs which resemble their counterparts in NS systems (Psaltis, Belloni & van der Klis 1999). Clearly, the magnetic warping and precession torques discussed in this paper are irrelevant to black hole systems⁸. We note that the phenomenology of black hole QPOs is much less developed, and that many of the \dot{M} -dependent behaviors of LFQPOs observed in NS systems are absent in the black hole systems (see Remillard 2001).

This work is supported in part by NSF Grant AST 9986740 and NASA grant NAG 5-8484, as well as by a research fellowship (to D.L.) from the Alfred P. Sloan foundation.

⁸Note that even without the magnetic torques and the classical precession, the mode frequency is reduced relative to the Lense-Thirring frequency at r_{in} as \dot{M} increases (see Fig. 3); this result applies equally to the black hole systems except that the mode is damped in the absence of other excitation mechanisms.

REFERENCES

- Alpar, M. A., & Shaham, J. 1985, *Nature*, 316, 239
- Bardeen, J. M., Press, W. H., & Teukolsky S. A. 1972, *ApJ*, 178, 347
- Bardeen, J. M., & Petterson, J. A. 1975, *ApJ*, 195, L65
- Cumming, A., Zweibel, E. G., & Bildsten L. 2001, *ApJ* submitted (astro-ph/0102178)
- Ford, E. C., & van der Klis, M. 1998, *ApJ*, 506, L39
- Homan, J., et al. 2001, *ApJ*, submitted (astro-ph/0104323)
- Jonker, P.G., et al. 2000, *ApJ*, 537, 374
- Lai, D., Rasio, F. A., & Shapiro, S. L. 1993, *ApJS*, 88, 205
- Lai, D., Rasio, F. A., & Shapiro, S. L. 1994, *ApJ*, 423, 344
- Lai, D., Lovelace, R., Wasserman, I. 1999, unpublished (astro-ph/9904111)
- Lai, D. 1998, *ApJ*, 502, 721
- Lai, D. 1999, *ApJ*, 524, 1030
- Lamb, F. K., Shibazaki, N., Alpar, M. A., & Shaham, J. 1985, *Nature*, 317, 681
- Marković, D., & Lamb, F. K. 1998, *ApJ*, 507, 316
- Morsink, S. M., & Stella, L. 1999, *ApJ*, 513, 827
- Ogilvie, G.I. 2000, *MNRAS*, 317, 607
- Ogilvie, G.I., & Dubus, G. 2001, *MNRAS*, 320, 485.
- Papaloizou, J. C., & Pringle, J. E. 1983, *MNRAS*, 202, 1181
- Press, W. H., Teukolsky, S., Vetterling, W. T., & Flannery, B. P. 1992, *Numerical Recipes* (Cambridge: Cambridge Univ. Press)
- Pringle, J. E. 1992, *MNRAS*, 258, 811
- Pringle, J. E. 1996, *MNRAS*, 281, 857
- Psaltis, D., et al. 1999, *ApJ*, 520, 763
- Psaltis, D., Belloni, T., & van der Klis, M. 1999, *ApJ*, 520, 262
- Remillard, R.A. 2001, in *Evolution of Binary and Multiple Stars*, eds. P. Podsiadlowski et al. (San Francisco: ASP), in press (astro-ph/0103431)
- Shakura, N. I., & Sunyaev, R. A. 1973, *A&A*, 24, 337
- Shirakawa, A., & Lai, D. 2001, *ApJ*, submitted (astro-ph/0109049)
- Stella, L., & Vietri, M. 1998, *ApJ*, 492, L59

- Strohmayer, T. E. 2001, *Advances in Space Research*, in press (astro-ph/0012516)
- Terquem, C. 1998, *ApJ*, 509, 819.
- van der Klis, M. 1995, in *X-Ray Binaries*, ed. W. H. G. Lewin, J. van Paradijs, & E. P. J. van den Heuvel (Cambridge: Cambridge Univ. Press), 252
- van der Klis, M. 2000, *ARAA*, 38, 717
- Wijnands, R. A. D. et al. 1996, *ApJ*, 469, L5
- Wijnands, R., & van der Klis, M. 1998 *Nature*, 394, 344

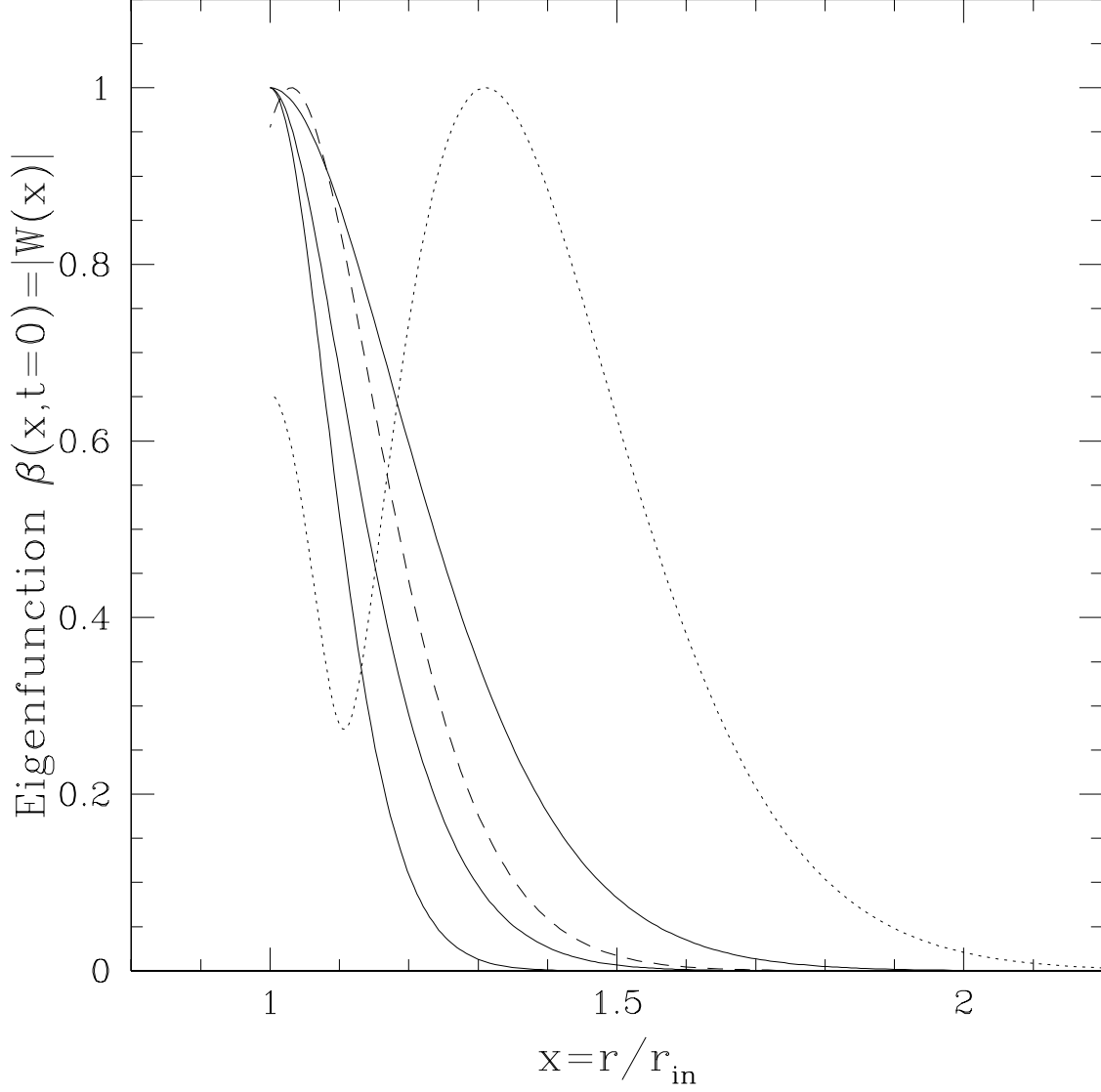


Fig. 1.— The disk tilt angle of the warping/precession modes for various parameter sets. The solid curves represent the fundamental modes for $(\hat{\Omega}_{LT}, \hat{\Gamma}_m) = (1000, 0)$, $(100, 100)$, and $(100, 0)$ (with $\hat{\Omega}_{cl} = \hat{\Omega}_m = 0$) from left to right, with the corresponding mode frequency $\hat{\sigma} = (\hat{\sigma}_r, \hat{\sigma}_i) = (860, 78)$, $(80, -46)$, and $(70, 15)$; the dotted curve represents a higher order mode for $(\hat{\Omega}_{LT}, \hat{\Gamma}_m) = (100, 100)$, with $\hat{\sigma} = (\hat{\sigma}_r, \hat{\sigma}_i) = (41, 6.0)$; all these are calculated using the inner boundary condition (B.C.) $W' = 0$. The dashed curve shows the case for $(\hat{\Omega}_{LT}, \hat{\Gamma}_m) = (100, 100)$, with the mode frequency $\hat{\sigma} = (65, -37)$, calculated using the inner B.C. $W' = W$. The eigenfunctions are normalized such that the maximum tilt angle is 1.

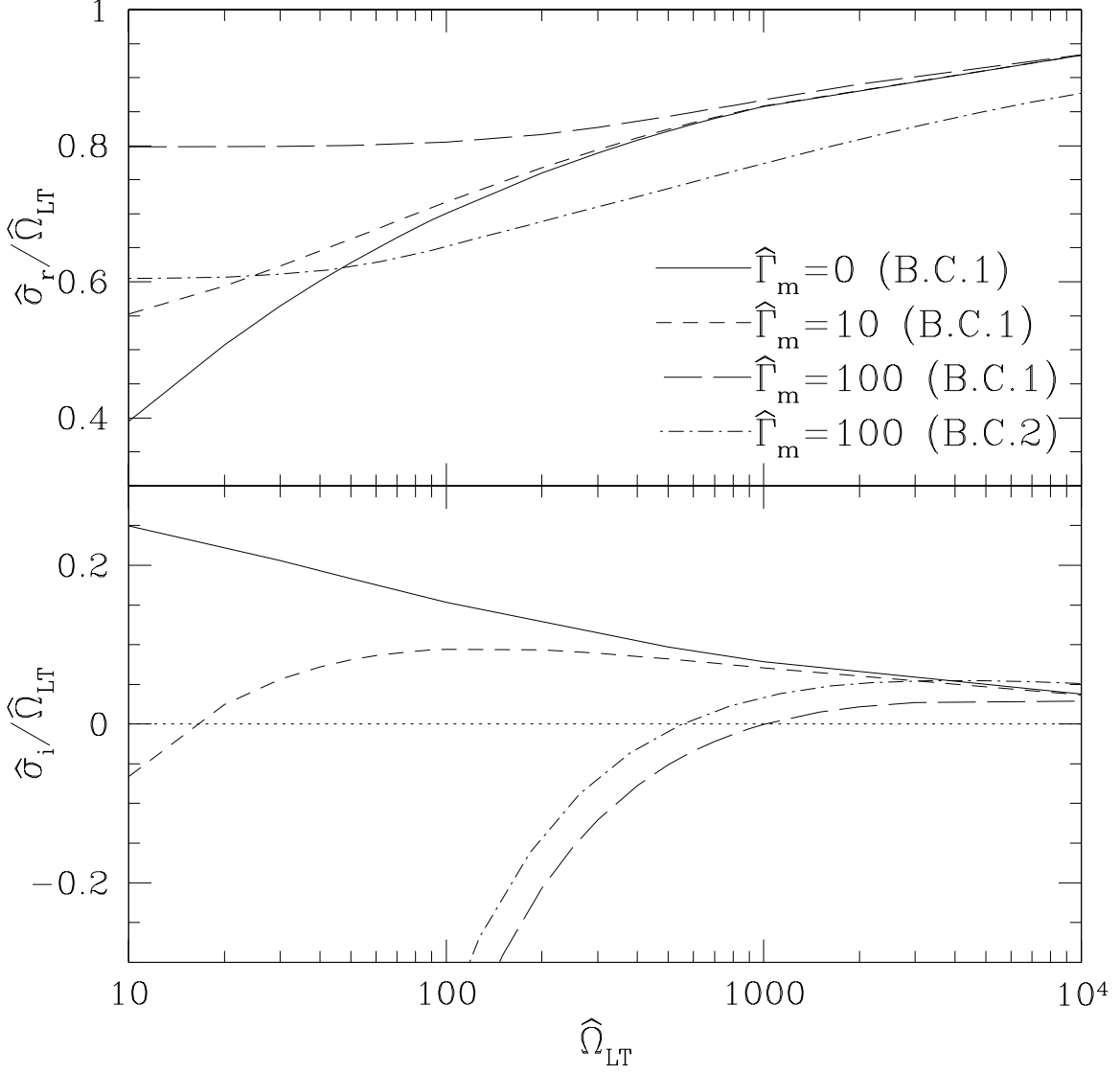


Fig. 2.— The upper panel shows the mode frequency $\hat{\sigma}_r$ in units of $\hat{\Omega}_{LT}$ as a function of $\hat{\Omega}_{LT}$ for different values of $\hat{\Gamma}_m$ (with $\hat{\Omega}_{cl} = \hat{\Omega}_m = 0$). The lower panel shows the corresponding mode damping rate $\hat{\sigma}_i$ (in units of $\hat{\Omega}_{LT}$). Note that negative $\hat{\sigma}_i$ implies growing mode. The dot-dashed curves are obtained using the inner boundary condition $W' = W$, while all other curves are based on B.C. $W' = 0$.

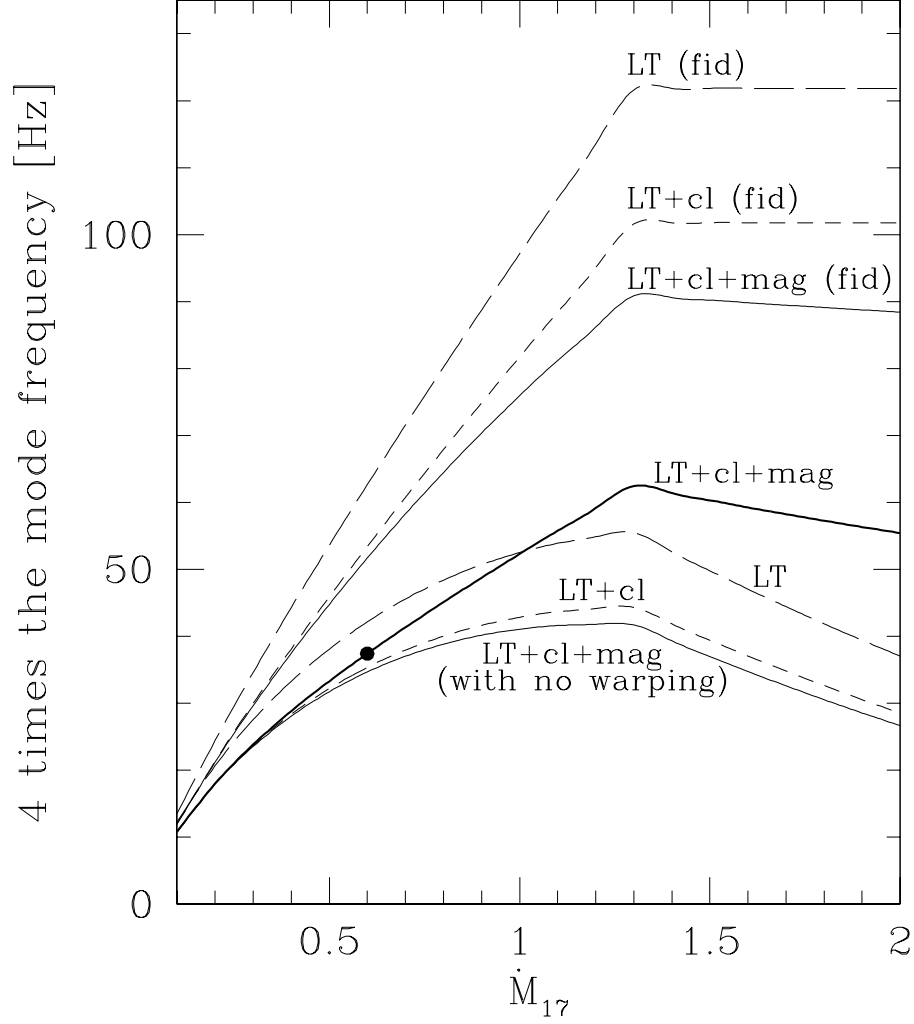


Fig. 3.— The global precession mode frequency $\sigma_r/2\pi$ as a function of the accretion rate \dot{M}_{17} . The frequencies are multiplied by 4 to facilitate comparison with observations (see the text for discussion). The upper three curves represent the fiducial frequency ν_{fid} for three different cases described in the text: (i) only the Lense-Thirring precession is included (long dashed curve), (ii) both the Lense-Thirring and classical precessions are included (short dashed curve), and (iii) the magnetic precession and warping are included as well as the Lense-Thirring and classical precessions (solid curve). The thick solid curve is the corresponding global precession frequency $\sigma_r/2\pi$ for case (iii) (Note that the modes grow above $\dot{M}_{17} \simeq 0.6$; marked by a dot in the figure). The lower two dashed curves are the corresponding global precession frequency $\sigma_r/2\pi$ for case (i) and (ii). The lower light solid curve shows $\sigma_r/2\pi$ for case (iii) obtained with the magnetic warping torque artificially turned off.

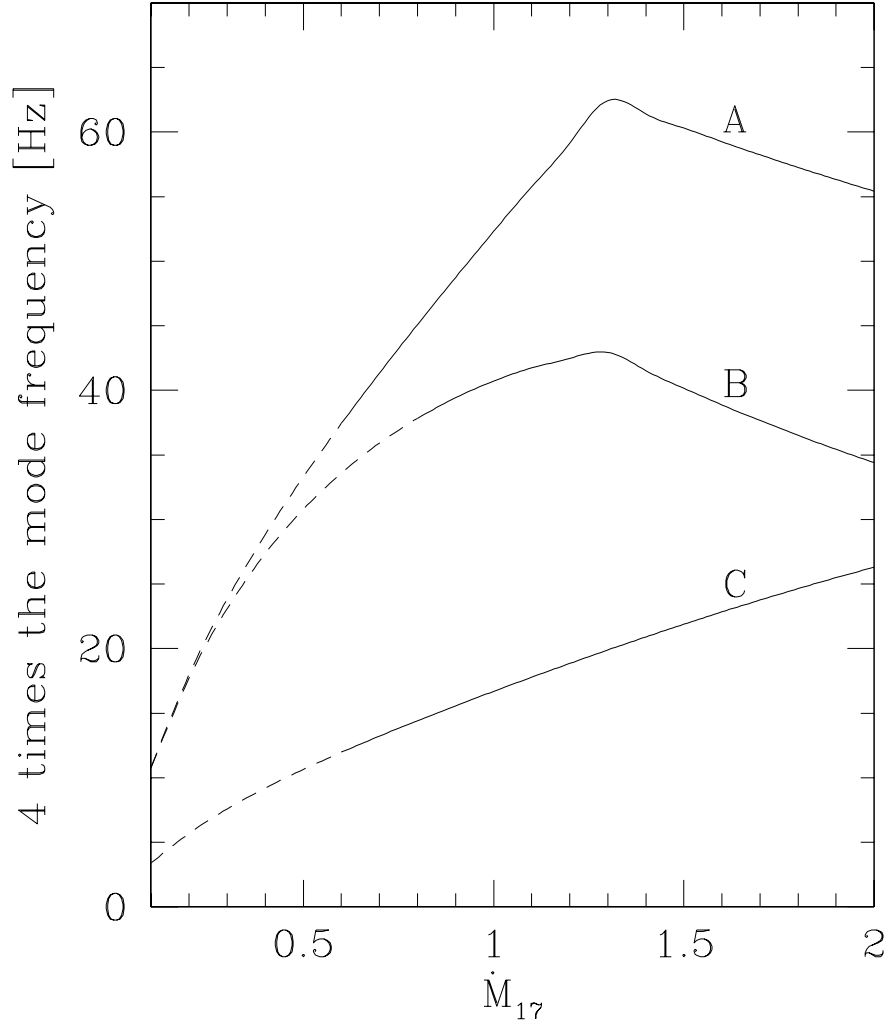


Fig. 4.— Correlation between the mode frequency $\sigma_r/2\pi$ and the accretion rate \dot{M}_{17} for Parameter Sets A, B, and C: $(\mu_{26}, \sin^2 \theta) = (2, 0.1)$, $(2, 0.5)$, & $(4, 0.1)$, respectively (see the text for the values of other fixed parameters) when all of the Lense Thirring, classical, and magnetic precessions and magnetic warping are taken into account. The solid portion of the curve corresponds to growing mode and the dashed portion corresponds to damping mode. To compare with LFQPOs observed in LMXBs, we multiply $\sigma_r/2\pi$ by 4.

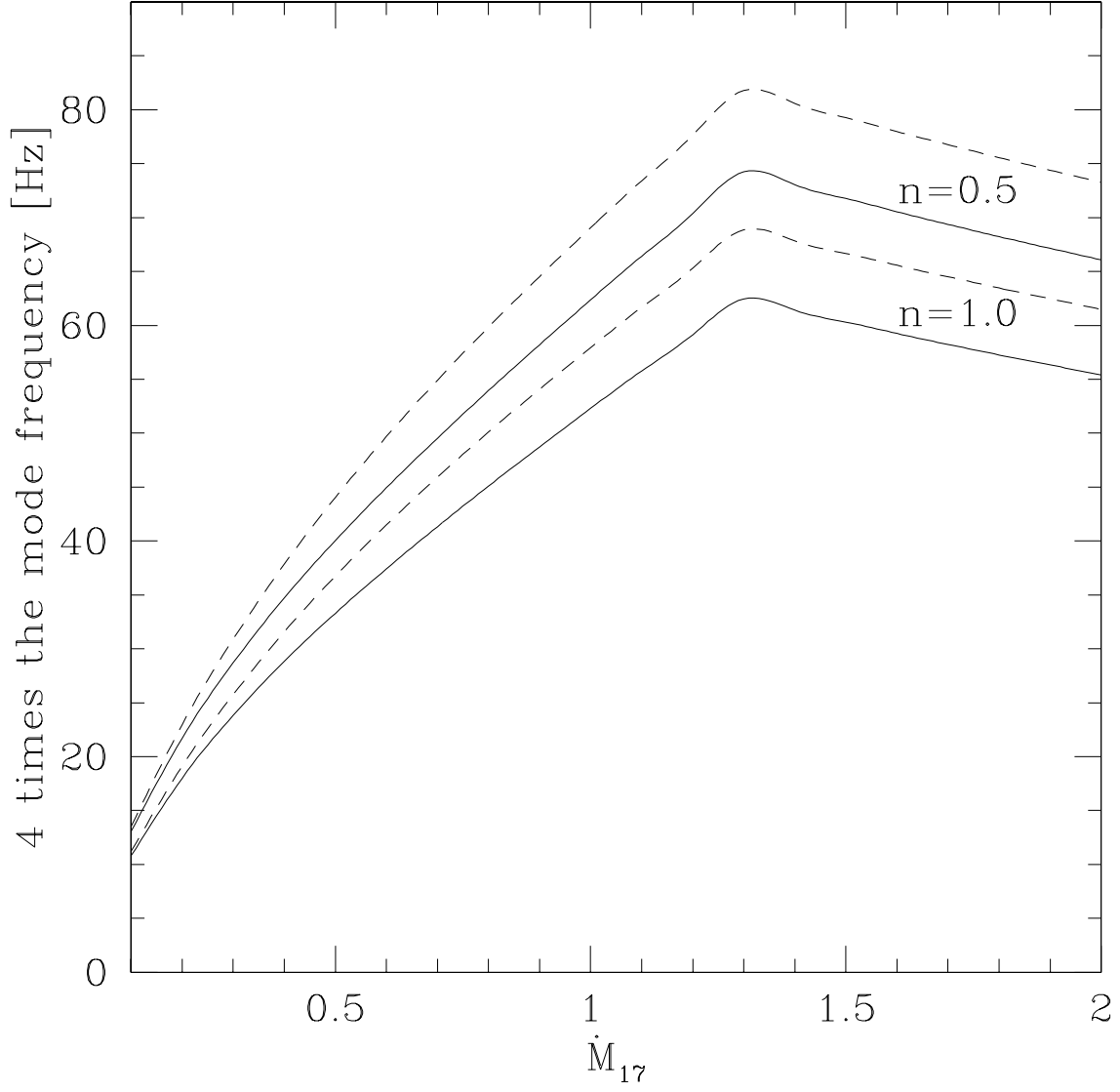


Fig. 5.— The mode frequency $\sigma_r/2\pi$ (multiplied by 4) as a function of \dot{M}_{17} for polytropic index $n = 0.5$ (upper two curves) and 1 (lower two curves), and for $\xi = 0$ (solid curves) and $\xi = 0.5$ (dashed curves) [see eq. (6)]. Other parameters are the same as in Parameter Set A adopted in Fig. 4.

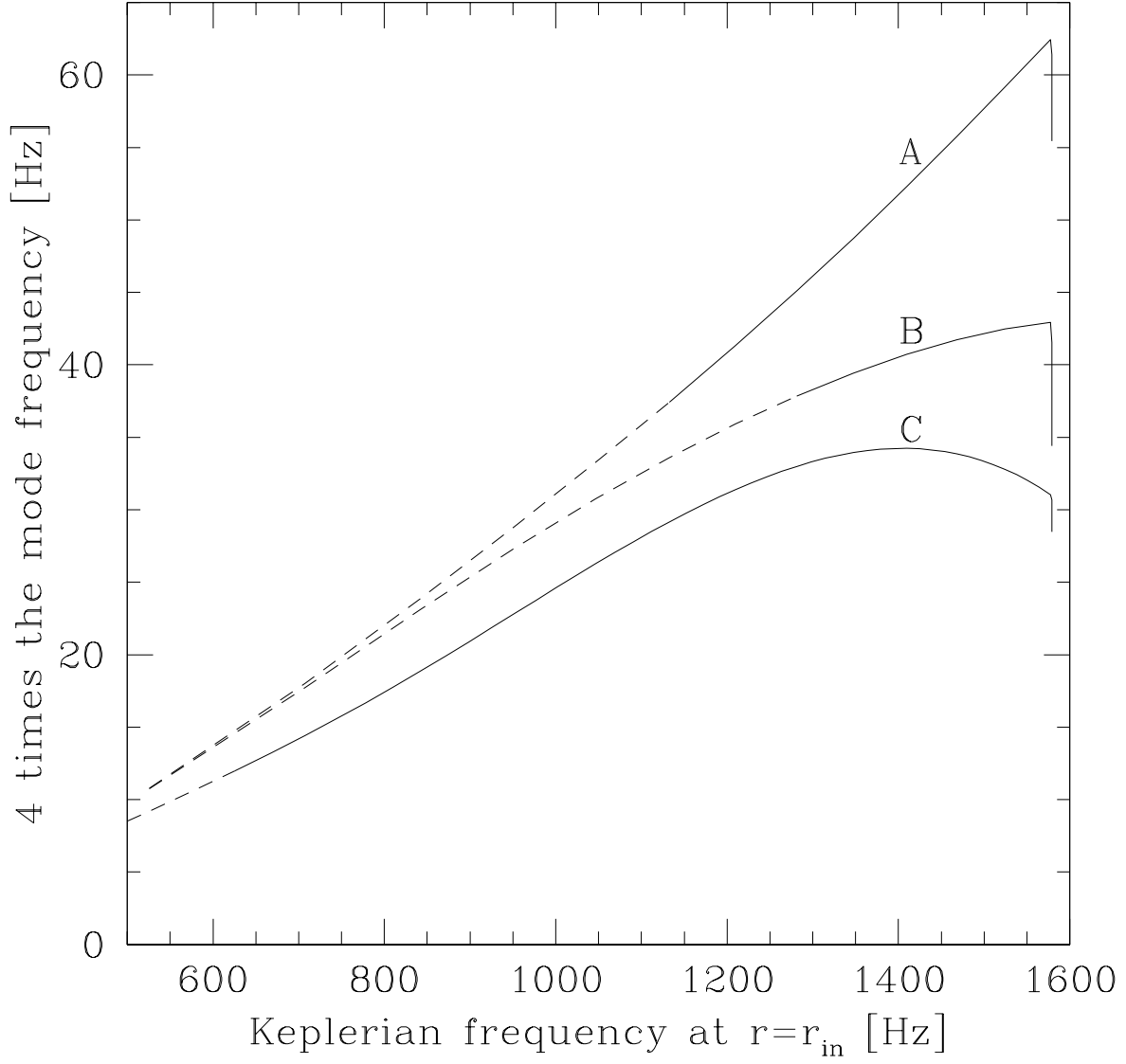


Fig. 6.— Correlation between the mode frequency $\sigma_r/2\pi$ (multiplied by 4) and the Keplerian frequency at the inner radius of the disk for Parameter Sets A, B, and C as in Fig. 4. The solid portion of the curve corresponds to growing mode and the dashed portion corresponds to damping mode.